CMS Physics Analysis Summary

Contact: cms-pag-conveners-susy@cern.ch 2016/08/04

Search for direct top squark pair production in the single lepton final state at $\sqrt{s} = 13$ TeV

The CMS Collaboration

Abstract

A search for direct top squark pair production in pp collisions at $\sqrt{s} = 13$ TeV is performed using events with a single isolated lepton, jets, and large transverse momentum imbalance. This analysis closely follows the strategy of a similar search for the same signature in 2015, using data collected in 2016 at a center-of-mass energy of 13 TeV with the CMS detector and corresponding to an integrated luminosity of 12.9 fb^{-1}. No significant excess in data is observed above the expectation from standard model processes. Exclusion limits are set in the context of supersymmetric models with pair production of top squarks that decay either to a top quark and a neutralino or to a bottom quark and a chargino.

1 Introduction

We present the result of a search for top squark pair production in a final state with a single lepton, jets, and significant transverse momentum imbalance. Searches for this signature were previously reported by the ATLAS [1] and CMS [2] collaborations using 13 TeV proton-proton (pp) collision data. This search is a continuation of previous work [2], performed using data from pp collisions collected during 2016 at a center-of-mass energy of 13 TeV with the Compact Muon Solenoid (CMS) detector at the LHC corresponding to an integrated luminosity of 12.9 fb^{-1}. We observe no evidence for an excess above the expected background from SM processes and interpret the results as limits on the production of pairs of top squarks for the different decay modes shown in Fig. 1.

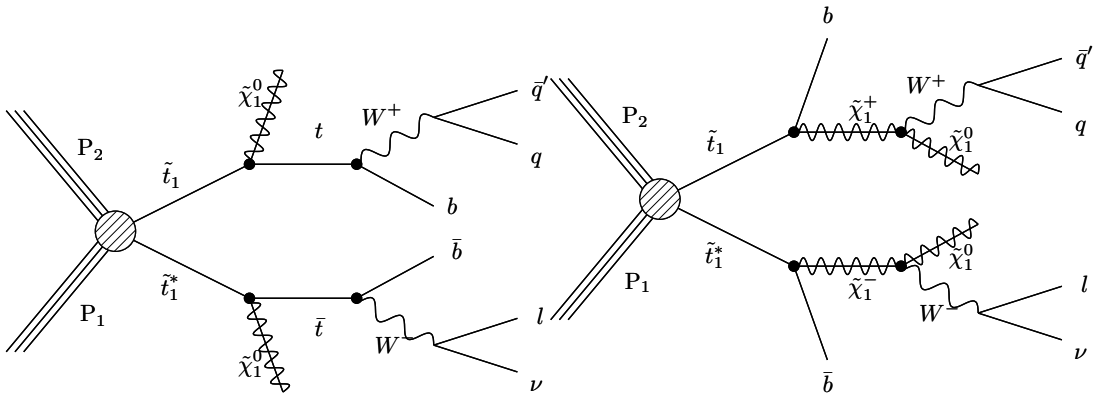

(a) $pp \to \tilde{t}_1\tilde{t}_1^* \to t^{(*)}\chi_1^0\bar{t}^{(*)}\chi_1^0$ (b) $pp \to \tilde{t}_1\tilde{t}_1^* \to b\chi_1^+\bar{b}\chi_1^-$

Figure 1: Diagrams for the pair production of top squarks corresponding to the different decay modes.

2 Event selection

This search is based on similar objects and calibrations as the 2015 analysis [2], and makes use of Monte Carlo (MC) samples produced with the same generator and simulation programs and processed with the same chain of reconstruction programs used for collision data. In the interest of brevity, we provide here only a short summary of the analysis, highlighting any changes made with respect to that performed on 2015 data.

2.1 Object definition and event preselection

The objects and pre-selection used here are identical to those in the previous version of this search [2]. Data events are selected using triggers that require either large missing transverse momentum, $E_{\mathrm{T}}^{\mathrm{miss}} > 100\,\mathrm{GeV}$ and $H_{\mathrm{T}}^{\mathrm{miss}} > 100\,\mathrm{GeV}$, or the presence of an isolated electron or muon with transverse momentum (p_{T}) thresholds of 25 GeV or 22 GeV, respectively. Here, the missing transverse momentum vector, $\vec{p}_{\mathrm{T}}^{\mathrm{miss}}$, is defined as the negative vector sum of the momentum of all reconstructed particles projected onto the plane perpendicular to the LHC beams. Its magnitude is referred to as $E_{\mathrm{T}}^{\mathrm{miss}}$. The observable $H_{\mathrm{T}}^{\mathrm{miss}}$ is the magnitude of $\vec{H}_{\mathrm{T}}^{\mathrm{miss}}$, the negative vectorial sum of the p_{T} of jets with $p_{\mathrm{T}} > 20\,\mathrm{GeV}$ in an event. The combined trigger efficiency, as measured with a data sample of events with large scalar sum of jet transverse momenta (H_T), is found to be $> 99\%$ with an uncertainty of 2-5%.

Selected events are required to have exactly one electron or muon with $p_{\mathrm{T}} > 20\,\mathrm{GeV}$ and $|\eta| < 2.4$ (1.442) for muons (electrons). Leptons are required to pass tight identification re-

quirements, be consistent with arising from the primary interaction vertex, and be isolated from other activity in the event. Typical lepton identification and isolation efficiencies are approximately 85% for electrons and 95% for muons, with variations at the level of a few percent depending on p_{T} and η.

Jets are formed by clustering particle-flow candidates using the anti-k_{T} algorithm [3] with a distance parameter of 0.4, and are corrected for contributions from pileup on an event-by-event basis using a jet area method [4]. Corrections are applied to the energy measurements of jets to account for non-uniform detector response and are propagated consistently as a correction to $\vec{p}_{\mathrm{T}}^{\,\mathrm{miss}}$. Jets overlapping with the selected lepton are not considered in the analysis.

Events are also required to contain at least two jets with $p_{\mathrm{T}} > 30\,\mathrm{GeV}$ and $|\eta| < 2.4$. One or more of these jets must be consistent with the decay of a heavy-flavor hadron, as identified using the medium operating point of the combined secondary vertex (CSVv2) tagging algorithm [5]. We refer to such jets as b-tagged jets. Finally the $E_{\mathrm{T}}^{\mathrm{miss}}$ is required to exceed 250 GeV. Events with possible contributions from beam halo processes or anomalous noise in the calorimeter are rejected using dedicated filters [6].

To suppress single-lepton backgrounds originating from semi-leptonic $\mathrm{t\bar{t}}$, W + jets, and single top processes, a requirement on the transverse mass of the lepton-neutrino system $M_{\mathrm{T}} = \sqrt{2p_{\mathrm{T}}^{\ell}E_{\mathrm{T}}^{\mathrm{miss}}(1-\cos(\phi))}$ is imposed, where ϕ is the angle between the transverse momentum of the lepton and $E_{\mathrm{T}}^{\mathrm{miss}}$. Background processes containing a single leptonically-decaying W boson have a kinematic endpoint $M_{\mathrm{T}} < M_{\mathrm{W}}$, modulo effects of the detector resolution and off-shell W mass effects. In this analysis we require $M_T > 150\,\mathrm{GeV}$, which significantly reduces single-lepton backgrounds. To further reduce the $\mathrm{t\bar{t}}$ background, we require the azimuthal angle between $\vec{p}_{\mathrm{T}}^{\,\mathrm{miss}}$ and the closest of the two leading E_{T} jets ($\Delta\phi$) to be larger than 0.8 radians.

The remaining background after these selections is dominated by dilepton events from $\mathrm{t\bar{t}}$ and tW production, where one of the leptons is not reconstructed or identified and the presence of the additional neutrino from the second leptonically-decaying W boson allows the event to pass the M_{T} requirement. In order to reduce this background, we relax the lepton relative isolation requirement to 0.2 to look for the presence of a second electron or muon with $p_{\mathrm{T}} > 5\,\mathrm{GeV}$, and reject an event if such a lepton is found. Moreover, an event is rejected if, in addition to the selected lepton, it contains a reconstructed hadronic tau lepton with $p_{\mathrm{T}} > 20\,\mathrm{GeV}$ or an isolated track with $p_{\mathrm{T}} > 10\,\mathrm{GeV}$.

2.2 Signal Region Definitions

Kinematic properties of signal events such as $E_{\mathrm{T}}^{\mathrm{miss}}$, M_{T}, and jet multiplicity depend on the decay modes of the top squarks, as well as on the mass splittings between the top squark, neutralino, and chargino (when present). To improve the sensitivity of this analysis, we optimized signal region selections separately for the different signal topologies shown in Fig. 1, and for several mass splitting regions. Search regions are defined similarly to those used in the previous version of this search, with a few additional bins at higher values of $E_{\mathrm{T}}^{\mathrm{miss}}$ added in this search to enhance sensitivity to a higher mass top squark.

Here, the $M_{\mathrm{T2}}^{\mathrm{W}}$ variable is defined according to [7], and the modified topness variable t_{mod} by:

$$t_{\mathrm{mod}} = \ln(\min S) \;\text{ with }\; S(\vec{p}_W, p_{\nu,z}) = \frac{(m_W^2 - (p_\nu + p_\ell)^2)^2}{a_W^4} + \frac{(m_t^2 - (p_b + p_W)^2)^2}{a_t^4}. \qquad (1)$$

Table 1: Summary of the signal region definitions.

N_{jets}	M_{T2}^{W} [GeV]	t_{mod}	$E_{\text{T}}^{\text{miss}}$ [GeV]				
$= 2$		> 6.4	250–350	350–450	> 450		
$= 3$	> 200		250–350	350–450	450–550	> 550	
≥ 4	≤ 200		250–350	350–450	> 450		
≥ 4	> 200		250–350	350–450	450–550	550–650	> 650

The topness variable used in this search is modified with respect to [8] by dropping the terms corresponding to the leptonic top quark decay and the center-of-mass energy. The calculation of modified topness in this analysis uses resolution parameters $a_W = 5\,\text{GeV}$ and $a_t = 15\,\text{GeV}$.

A summary of all search regions is given in Table 1.

3 Background estimation

Three categories of backgrounds originating from SM processes remain after the preselection described in Section 2. The dominant contribution arises from SM backgrounds where one of the leptons is not reconstructed or identified. These events are classified as "lost lepton" events and they come primarily from $\text{t}\bar{\text{t}} \to 2\ell$. We estimate this background using a dilepton control region.

A second class of background events comes from SM processes with a single leptonically decaying W boson. Preselection requirements of $E_{\text{T}}^{\text{miss}} > 250\,\text{GeV}$ and $M_{\text{T}} > 150\,\text{GeV}$ strongly suppress this background. The suppression is much stronger for events with W boson originating from the decay of a top quark than for direct W boson production, as the mass of the top quark imposes a bound on M_{W}. As a result, the tail of the M_{T} distribution in semi-leptonic $\text{t}\bar{\text{t}}$ events is dominated by $E_{\text{T}}^{\text{miss}}$ resolution effects, while for events where the W is produced directly (W+jets) it is largely driven by the width of the W boson.

In the search regions where the contribution from W+jets is significant, we estimate it using a control region with zero b-tagged jets; simulation is used in the remaining regions. The subleading semi-leptonic $\text{t}\bar{\text{t}} \to 1\ell$ background is modeled by using simulated events.

The third class of background events includes rare SM processes such as WZ and $\text{t}\bar{\text{t}}\text{Z}$ (where the Z boson decays to neutrinos), with smaller contributions from $\text{t}\bar{\text{t}}\text{W}$, $\text{t}\bar{\text{t}}\gamma$, and processes with two or three electroweak vector bosons. These backgrounds are estimated by using simulated events. Multijet background is negligible in this search due to the requirements of a high-p_{T} isolated lepton, large $E_{\text{T}}^{\text{miss}}$, and large M_{T}.

3.1 Lost lepton background

The lost lepton background is estimated from a dilepton control region using a transfer factor obtained from simulated samples. One control region is defined for each signal region, with the same requirements except for requiring the presence of a second lepton with $p_{\text{T}} > 10\,\text{GeV}$ passing the veto requirements. In each dilepton control region, we remove the trailing lepton from the event by adding its p_{T} to the $E_{\text{T}}^{\text{miss}}$ and recalculate all relevant event quantities. The transfer factor accounts for the lepton acceptance and the efficiency of the lepton reconstruction, identification, and isolation. Corrections obtained from tag-and-probe measurements in samples of $\text{Z}/\gamma^\star \to \ell\ell$ events account for observed differences in lepton reconstruction and selection efficiencies between data and simulation.

The dominant uncertainties on the transfer factor come from the statistical uncertainty on the MC and the uncertainties on the lepton scale factors, which can reach up to 15% and 10%, respectively. Uncertainties in the jet energy scale, b-tagging scale factors, and renormalization and factorization scale are found to be small, resulting in a total systematic uncertainty of less than 20%, which is smaller than the statistical uncertainty from the data yields in the control sample in nearly all regions. Table 2 shows the yields in the data control regions and the transfer factors used in the extrapolation. The final column shows the estimated number of events in our signal regions and the total systematic in the estimate.

Table 2: Event yields in data control regions for the lost lepton background and the transfer factor. The last column shows the final background estimate, including all systematic uncertainties.

$E_{\mathrm{T}}^{\mathrm{miss}}$ [GeV]	Control region data	Transfer factor	$N_{2\ell}^{est,SR}$
	2 jets, t_{mod} >6.4		
$250 < E_{\mathrm{T}}^{\mathrm{miss}} < 350\,\mathrm{GeV}$	164	0.24 ± 0.02	39.1 ± 5.0
$350 < E_{\mathrm{T}}^{\mathrm{miss}} < 450\,\mathrm{GeV}$	33	0.18 ± 0.03	6.1 ± 1.5
$E_{\mathrm{T}}^{\mathrm{miss}} > 450\,\mathrm{GeV}$	7	0.07 ± 0.01	0.46 ± 0.19
	3 jets, $M_{\mathrm{T2}}^{\mathrm{W}}$ >200 GeV		
$250 < E_{\mathrm{T}}^{\mathrm{miss}} < 350\,\mathrm{GeV}$	77	0.29 ± 0.03	22.7 ± 3.4
$350 < E_{\mathrm{T}}^{\mathrm{miss}} < 450\,\mathrm{GeV}$	29	0.20 ± 0.02	589 ± 1.2
$450 < E_{\mathrm{T}}^{\mathrm{miss}} < 550\,\mathrm{GeV}$	19	0.13 ± 0.02	2.5 ± 0.7
$E_{\mathrm{T}}^{\mathrm{miss}} > 550\,\mathrm{GeV}$	19	0.07 ± 0.01	1.3 ± 0.4
	$\geq$4 jets, $M_{\mathrm{T2}}^{\mathrm{W}}$ $\leq$200 GeV		
$250 < E_{\mathrm{T}}^{\mathrm{miss}} < 350\,\mathrm{GeV}$	254	0.49 ± 0.04	125 ± 13
$350 < E_{\mathrm{T}}^{\mathrm{miss}} < 450\,\mathrm{GeV}$	59	0.40 ± 0.03	23.6 ± 3.7
$E_{\mathrm{T}}^{\mathrm{miss}} > 450\,\mathrm{GeV}$	15	0.38 ± 0.04	5.7 ± 1.6
	$\geq$4 jets, $M_{\mathrm{T2}}^{\mathrm{W}}$ >200 GeV		
$250 < E_{\mathrm{T}}^{\mathrm{miss}} < 350\,\mathrm{GeV}$	87	0.34 ± 0.03	29.3 ± 4.2
$350 < E_{\mathrm{T}}^{\mathrm{miss}} < 450\,\mathrm{GeV}$	24	0.32 ± 0.03	7.8 ± 1.8
$550 < E_{\mathrm{T}}^{\mathrm{miss}} < 550\,\mathrm{GeV}$	11	0.32 ± 0.04	3.5 ± 1.1
$550 < E_{\mathrm{T}}^{\mathrm{miss}} < 650\,\mathrm{GeV}$	4	0.26 ± 0.05	1.0 ± 0.5
$E_{\mathrm{T}}^{\mathrm{miss}} > 650\,\mathrm{GeV}$	4	0.09 ± 0.02	0.37 ± 0.20

3.2 One lepton background

In the signal regions with high $M_{\mathrm{T2}}^{\mathrm{W}}$ or the modified topness requirement, the W + jets background is estimated using data events containing no b-tagged jets. For low $M_{\mathrm{T2}}^{\mathrm{W}}$ regions, this process contributes less than 10% to the total background and thus we do not employ a data-driven method, but instead use the predictions from MC simulation. Also the background from $\mathrm{t\bar{t}} \to 1\ell$, which is heavily suppressed by the $E_{\mathrm{T}}^{\mathrm{miss}}$ and M_{T} requirements, is estimated by using simulated events.

For the signal regions targeting scenarios with a large mass splitting between the top squark and the LSP, we estimate the W + jets background in a manner analogous to the lost lepton background described above. One control region is defined for each signal region, with the same requirements except for requiring 0 b-tagged jets. At high M_{T}, approximately 25-35% of the control region yield is expected to be from dileptonic $\mathrm{t\bar{t}}$ and invisible Z processes. The control region yield is corrected by multiplying by the expected purity obtained from simulation

with a 50% uncertainty on the non-one lepton contribution.

The expected contribution in the signal region is extrapolated from the corrected control region yield using a transfer factor obtained from simulation, which accounts for b quark acceptance and tagging efficiency and is corrected for measured differences in the performance of the b-tagging algorithm between data and simulation.

The largest uncertainty on this transfer factor comes from MC statistics, followed by the uncertainty on the heavy-flavor component of the W + jets cross section. A comparison of the N_b distribution between data and simulation is performed in a W + jets enriched region by selecting events with 1 or 2 jets and $E_T^{miss} > 50$ GeV. Figure 2 shows that the difference observed between data and simulation is well within the 50% uncertainty on the heavy-flavor component, indicated by the shaded band. Variations of the jet energy scale and b-tagging scale factors within their measured uncertainties each result in a 10% uncertainty on the background estimate. The total uncertainty on the W + jets estimate varies from 20% to 80%.

The background yields for the one-lepton backgrounds are summarized in Table 3. The observed yields in the data control regions and the transfer factors used are also listed together with the systematic uncertainties on the estimated signal yields.

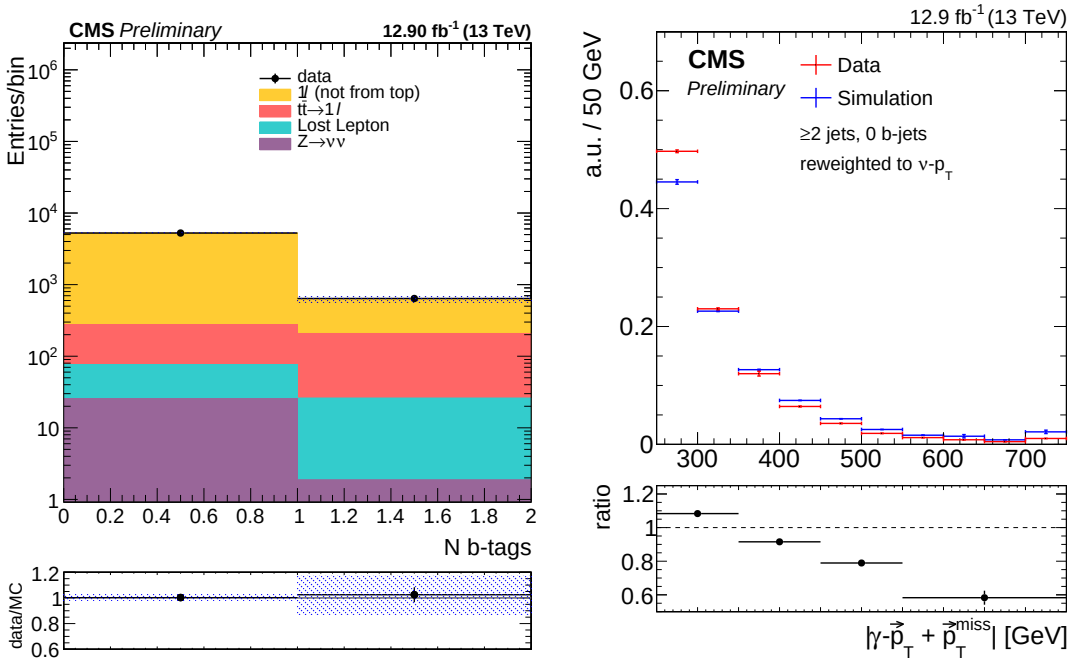

Figure 2: Left: Number of b-tagged jets distribution in a control sample with 1 or 2 jets and $E_T^{miss} > 250$ GeV. The shaded band shows the uncertainty applied due to a 50% systematic uncertainty on the heavy flavor component of the W+jets sample. Data and simulation agree well within uncertainties. Right: Comparison of the E_T^{miss} distribution between data and simulation in the γ+jets control region.

Studies with simulation indicate that the contribution from $t\bar{t} \to 1\ell$ is never larger than 10% of the total background. This estimate depends strongly on the correct modeling of the E_T^{miss} resolution in the detector simulation, as resolution effects enhance the M_T tail. The modeling of the E_T^{miss} resolution is studied by comparing a γ+jets sample in data and simulated events. The photon p_T spectrum is reweighted to match that of the neutrino in the simulated $t\bar{t} \to 1\ell$ sam-

ple. We then add the photon p_T to the E_T^{miss} and compare the resulting spectrum. Differences of up to 40% in the E_T^{miss} shape between data and simulated events are observed, as shown in Fig. 2 (right) for a selection with at least 2 jets. Corrections for these differences are applied to the $t\bar{t} \to 1\ell$ simulation and a resulting 100% uncertainty is assigned to the estimate of the background.

Table 3: Event yields in the W+jets 0 b-tagged control region and the transfer factors used to estimate the W+jets background. The final W+jets yields and the $t\bar{t} \to 1\ell$ estimate from simulation with their combined systematic and statistical uncertainty are shown in the last two colums for $\mathcal{L}$ of data. The low ΔM regions are fully estimated from simulation. For the transfer factors only the statistical uncertainty is shown.

E_T^{miss} [GeV]	Control region data	Transfer factor	$N_{WJets}^{est,SR}$	$t\bar{t} \to 1\ell$
	2 jets, t_{mod} >6.4			
250<E_T^{miss} <350 GeV	246	0.088 ± 0.006	16.5 ± 3.3	0.42 ± 0.42
350<E_T^{miss} <450 GeV	86	0.079 ± 0.004	5.1 ± 1.2	—
E_T^{miss} >450 GeV	44	0.079 ± 0.008	2.7 ± 0.8	—
	3 jets, M_{T2}^W >200 GeV			
250<E_T^{miss} <350 GeV	106	0.16 ± 0.01	12.0 ± 3.0	0.16 ± 0.16
350<E_T^{miss} <450 GeV	36	0.13 ± 0.01	3.5 ± 0.9	—
450<E_T^{miss} <550 GeV	11	0.23 ± 0.06	2.0 ± 0.9	—
E_T^{miss} <550 GeV	14	0.16 ± 0.02	1.5 ± 0.6	—
	≥4 jets, M_{T2}^W ≤200 GeV			
250<E_T^{miss} <350 GeV	—	—	5.6 ± 5.6	6.6 ± 6.6
350<E_T^{miss} <450 GeV	—	—	1.1 ± 1.1	1.0 ± 1.0
E_T^{miss} >450 GeV	—	—	0.30 ± 0.30	0.32 ± 0.32
	≥4 jets, M_{T2}^W >200 GeV			
250<E_T^{miss} <350 GeV	52	0.26 ± 0.03	7.6 ± 3.3	2.8 ± 2.8
350<E_T^{miss} <450 GeV	21	0.25 ± 0.03	3.3 ± 1.3	0.97 ± 0.97
450<E_T^{miss} <550 GeV	2	0.24 ± 0.03	0.34 ± 0.25	0.04 ± 0.04
550<E_T^{miss} <650 GeV	4	0.20 ± 0.03	0.48 ± 0.31	—
E_T^{miss} >650 GeV	2	0.19 ± 0.04	0.23 ± 0.19	0.11 ± 0.11

3.3 Rare Standard Model backgrounds

The last category of background arises primarily from SM processes containing one or more Z bosons decaying to neutrinos, including $t\bar{t}$ production in association with a vector boson and diboson and triboson events. Within this category, WZ events dominate in the signal regions with two jets. In events with higher jet multiplicity, around 60–80% of the rare background is due to $t\bar{t}Z$ with the Z boson decaying into a pair of neutrinos ($Z \to \nu\bar{\nu}$). This fraction increases with a tighter E_T^{miss} requirement. Potential control regions, such as a trilepton final state, suffer from a limited number of events with the current amount of data. Therefore, the rare backgrounds are estimated by using simulated events. We assess all relevant theoretical and experimental uncertainties, the largest contributions coming from variations of the renormalization and factorization scales and the jet energy scale. The total uncertainty on the rare background ranges from 25-65%, depending on the signal region.

4 Results and interpretation

The data observed in the 15 search regions are statistically compatible with the estimated backgrounds from SM processes. Table 4 summarizes the results. The results of the search are interpreted in the context of the models of top squark pair production described in Section 1.

Table 4: Results of the data- and simulation-driven background estimates together with the observed data yields collected during 2016 pp collisions. The uncertainties are the quadratic sums of statistical and systematic uncertainties.

$E_{\mathrm{T}}^{\mathrm{miss}}$ [GeV]	Lost Lepton	1ℓ (not from top)	$\mathrm{t\bar{t}} \to 1\ell$	$\mathrm{Z} \to \nu\overline{\nu}$	Total background	Data
	2 jets, $t_{\mathrm{mod}} > 6.4$					
$250-350$	39.1 ± 5.0	16.5 ± 3.3	0.42 ± 0.42	2.6 ± 0.7	58.6 ± 6.0	72
$350-450$	6.1 ± 1.5	5.1 ± 1.2	—	1.1 ± 0.4	12.2 ± 1.9	7
>450	0.46 ± 0.19	2.7 ± 0.8	—	0.52 ± 0.17	3.7 ± 0.8	5
	3 jets, $M_{\mathrm{T2}}^{\mathrm{W}} > 200\,\mathrm{GeV}$					
$250-350$	22.7 ± 3.4	12.0 ± 3.0	0.16 ± 0.16	3.1 ± 1.0	38.0 ± 4.6	35
$350-450$	5.8 ± 1.2	3.5 ± 0.9	—	1.2 ± 0.4	10.4 ± 1.6	9
$450-550$	2.5 ± 0.7	2.0 ± 0.9	—	0.76 ± 0.25	5.3 ± 1.1	6
>550	1.3 ± 0.4	1.5 ± 0.6	—	0.25 ± 0.09	3.0 ± 0.7	3
	≥ 4 jets, $M_{\mathrm{T2}}^{\mathrm{W}} \leq 200\,\mathrm{GeV}$					
$250-350$	125 ± 13	5.6 ± 5.6	6.6 ± 6.6	3.8 ± 1.5	141 ± 15	121
$350-450$	23.6 ± 3.7	1.1 ± 1.1	1.0 ± 1.0	0.89 ± 0.38	26.6 ± 4.0	22
>450	5.7 ± 1.6	0.30 ± 0.30	0.32 ± 0.32	0.25 ± 0.12	6.6 ± 1.6	9
	≥ 4 jets, $M_{\mathrm{T2}}^{\mathrm{W}} > 200\,\mathrm{GeV}$					
$250-350$	29.3 ± 4.2	7.6 ± 3.3	2.8 ± 2.8	3.6 ± 1.4	43.3 ± 6.2	44
$350-450$	7.8 ± 1.8	3.3 ± 1.3	0.97 ± 0.97	2.2 ± 0.8	14.2 ± 2.5	11
$450-550$	3.5 ± 1.1	0.34 ± 0.25	0.04 ± 0.04	0.86 ± 0.43	4.8 ± 1.3	5
$550-650$	1.0 ± 0.5	0.48 ± 0.31	—	0.19 ± 0.10	1.7 ± 0.6	1
>650	0.37 ± 0.20	0.23 ± 0.19	0.11 ± 0.11	0.21 ± 0.13	0.92 ± 0.33	3

For a given signal scenario, limits are derived by combining the regions defined in the first three rows of Table 1. When interpreting the scenario shown in Fig. 1a, the regions listed in the last row of Table 1 are used instead. The signal yield is corrected for signal contamination to the data control regions for each mass hypothesis. Typical values are around $5-10\%$, although for compressed $\Delta M(\tilde{\mathrm{t}}_1, \tilde{\chi}_1^0)$ it may reach up to 25%.

A summary of the uncertainties considered are shown in Table 5. The largest ones come from the limited size of the MC samples, b-tagging efficiency and jet energy scale, and for model points with small mass splittings, the recoil ISR uncertainty [9]. Additionally, as new physics signals are simulated using the CMS fast simulation package [10], an additional uncertainty is taken to cover potential differences in $E_{\mathrm{T}}^{\mathrm{miss}}$ resolution between this simulation and the full Geant4-based model [11] of the CMS detector. This uncertainty is small in the bulk of the signal scan, but may reach up to 25% in scenarios with a compressed mass spectrum. Uncertainties due to luminosity, ISR recoil, MET resolution, and b-tagging and lepton efficiencies are treated as correlated across search regions. No additional uncertainty from variations of the PDF set is taken as it is found to be mostly redundant with the recoil ISR uncertainty.

Figure 4 shows the 95% confidence level (CL) upper limit for $\mathrm{pp} \to \tilde{\mathrm{t}}_1\tilde{\mathrm{t}}_1^* \to \mathrm{t}^{(*)}\bar{\mathrm{t}}^{(*)}\tilde{\chi}_1^0\tilde{\chi}_1^0$, assuming the top squarks to be unpolarized, together with the upper limit at 95% CL on the signal

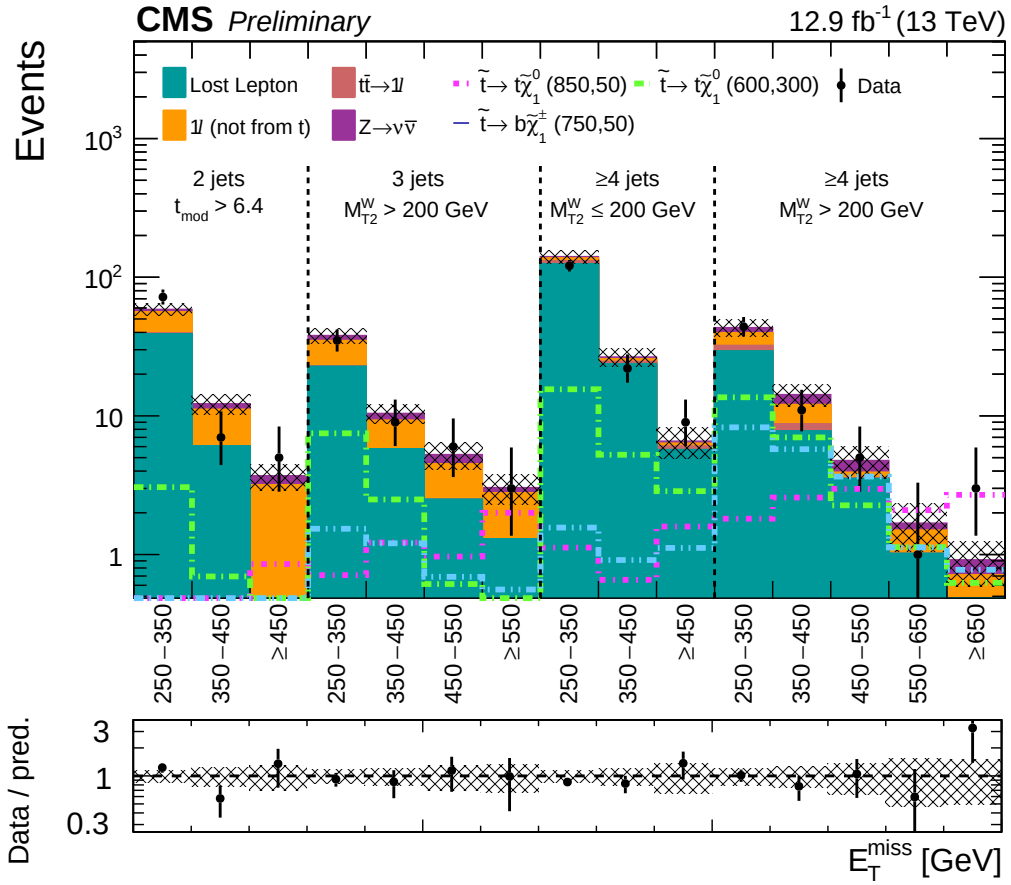

Figure 3: Data- and simulation-driven background estimates together with the observed data yields in the signal regions, described in Table 1, collected during 2016 pp collisions. The uncertainties, which are the quadratic sums of statistical and systematic uncertainties, are shown as shaded band. Three signal hypotheses are overlaid.

cross section. We exclude top squark masses up to 860 GeV for a massless LSP and LSP masses up to 380 GeV for a 700 GeV top squark mass.

Figure 5 shows the 95% confidence level (CL) upper limit for $pp \to \tilde{t}_1\tilde{t}_1^* \to b\bar{b}\tilde{\chi}_1^{\pm}\tilde{\chi}_1^{\pm}$, $\tilde{\chi}_1^{\pm} \to W\tilde{\chi}_1^0$, together with the upper limit at 95% CL on the excluded signal cross section. The mass of the chargino is chosen to be $(m_{\tilde{t}_1} + m_{\tilde{\chi}_1^0})/2$. We exclude top squark masses up to 775 GeV for a massless LSP and LSP masses up to 325 GeV for a 700 GeV top squark mass.

5 Summary

We presented a search for direct top squark pair production in pp collisions at $\sqrt{s} = 13\,\text{TeV}$ in events a single isolated charged electron of muon, jets, and large $E_{\text{T}}^{\text{miss}}$ using 12.9 fb^{-1} of data collected with the CMS detector during the 2016 run of the LHC. No sign of signal is observed and exclusion limits are set in the context of supersymmetric models with pair production of top squarks that decay either to a top quark and a neutralino or to a bottom quark and a chargino. Assuming that all top squarks decay to a top quark and a neutralino, we exclude at the 95% confidence level top squark masses up to 860 GeV for a massless neutralino and neutralino masses up to 380 GeV for a 700 GeV top squark mass. We also show results for the top squark decay to a top quark and a neutralino or a b quark and a chargino, with the chargino

Table 5: Summary of the systematic uncertainties for the signal and background estimates with their typical values in individual signal regions.

Source	Typical range of values
Simulation statistical uncertainty	3–35%
Renormalization and factorization scale	1–5%
Luminosity	6.2%
Trigger	2–5%
b-tagging scale factors	1–7%
Jet energy scale	1–20%
Lepton identification and veto efficiency	1–3%
System recoil("ISR")	2–20%
$E_{\mathrm{T}}^{\mathrm{miss}}$ modeling uncertainty	1–25%

mass being the average of the neutralino mass and top squark mass. In that scenario, we exclude at the 95% confidence level top squark masses up to 775 GeV for a massless neutralino and neutralino masses up to 325 GeV for a 700 GeV top squark mass.

References

[1] ATLAS Collaboration, "Search for top squarks in final states with one isolated lepton, jets, and missing transverse momentum in $\sqrt{s} = 13$ TeV pp collisions with the ATLAS detector", arXiv:1606.03903.

[2] CMS Collaboration, "Search for direct top squark pair production in the single lepton final state at $\sqrt{s} = 13$ TeV", Technical Report CMS-PAS-SUS-16-002, CERN, Geneva, 2016.

[3] M. Cacciari, G. P. Salam, and G. Soyez, "The anti-k_{T} jet clustering algorithm", *JHEP* **04** (2008) 063, doi:10.1088/1126-6708/2008/04/063, arXiv:0802.1189.

[4] M. Cacciari and G. P. Salam, "Pileup subtraction using jet areas", *Phys. Lett. B* **659** (2008) 119, doi:10.1016/j.physletb.2007.09.077, arXiv:0707.1378.

[5] CMS Collaboration, "Identification of b-quark jets with the CMS experiment", *JINST* **8** (2013) P04013, doi:10.1088/1748-0221/8/04/P04013, arXiv:1211.4462.

[6] CMS Collaboration, "Missing transverse energy performance of the CMS detector", *JINST* **6** (2011) P09001, doi:10.1088/1748-0221/6/09/P09001, arXiv:1106.5048.

[7] Y. Bai, H.-C. Cheng, J. Gallicchio, and J. Gu, "Stop the Top Background of the Stop Search", *JHEP* **07** (2012) 110, doi:10.1007/JHEP07(2012)110, arXiv:1203.4813.

[8] M. L. Graesser and J. Shelton, "Hunting Mixed Top Squark Decays", *Phys. Rev. Lett.* **111** (2013) 121802, doi:10.1103/PhysRevLett.111.121802, arXiv:1212.4495.

[9] CMS Collaboration, "Searches for third-generation squark production in fully hadronic final states in proton-proton collisions at $\sqrt{s} = 8$ TeV", *JHEP* **06** (2015) 116, doi:10.1007/JHEP06(2015)116, arXiv:1503.08037.

[10] S. Abdullin et al., "The fast simulation of the CMS detector at LHC", *J. Phys. Conf. Ser.* **331** (2011) 032049, doi:10.1088/1742-6596/331/3/032049.

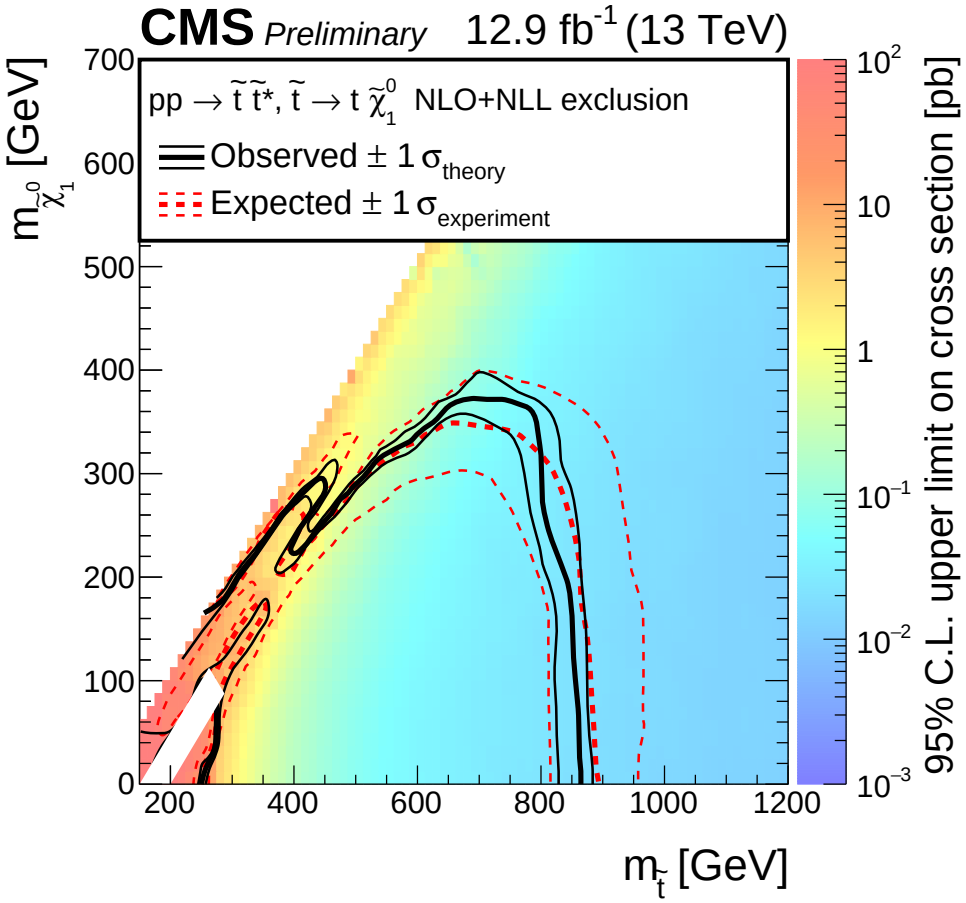

Figure 4: The exclusion limits at 95% CL for direct top-squark production with decay $\tilde{t}_1 \to t\tilde{\chi}_1^0$. The interpretation is done in the two dimensional space of $m_{\tilde{t}_1}$ vs. $m_{\tilde{\chi}_1^0}$. The color indicates the upper limit (95% CL) on the cross section times branching fraction at each point in the $m_{\tilde{t}_1}$ vs. $m_{\tilde{\chi}_1^0}$ plane. The area to the left of and below the thick black curve represents the observed exclusion region at 95% CL, while the dashed red lines indicate the expected limit at 95% CL and their $\pm 1\sigma$ experiment standard deviation uncertainties. The thin black lines show the effect of the theoretical uncertainties σ_{theory} on the signal cross section.

[11] GEANT4 Collaboration, "GEANT4—a simulation toolkit", *Nucl. Instrum. Meth. A* **506** (2003) 250, doi:10.1016/S0168-9002(03)01368-8.

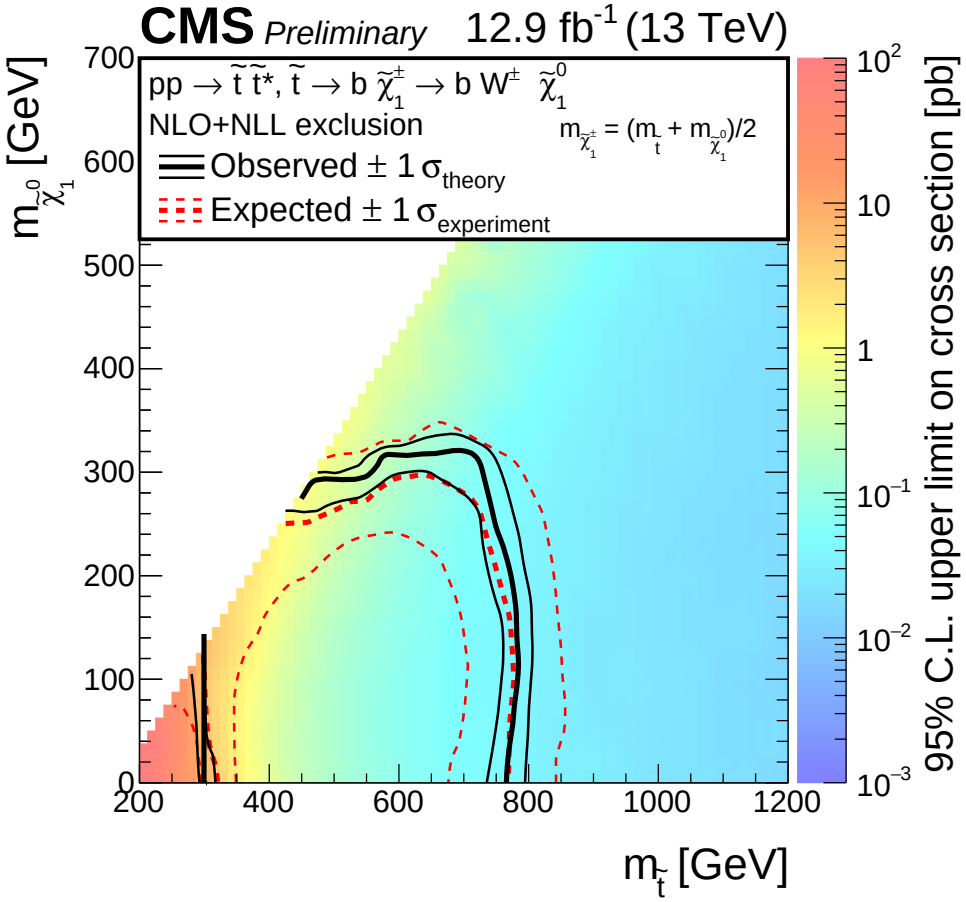

Figure 5: The exclusion limit at 95% CL for direct top-squark production with decay $pp \to \tilde{t}_1\tilde{t}_1^* \to b\bar{b}\tilde{\chi}_1^{\pm}\tilde{\chi}_1^{\pm}$, $\tilde{\chi}_1^{\pm} \to W\tilde{\chi}_1^0$. The mass of the chargino is chosen to be $(m_{\tilde{t}_1} + m_{\tilde{\chi}_1^0})/2$. The interpretation is done in the two dimensional space of $m_{\tilde{t}_1}$ vs. $m_{\tilde{\chi}_1^0}$. The color indicates the upper limit (95% CL) on the cross section times branching fraction at each point in the $m_{\tilde{t}_1}$ vs. $m_{\tilde{\chi}_1^0}$ plane. The area to the left of and below the thick black curve represents the observed exclusion region at 95% CL, while the dashed red lines indicate the expected limit at 95% CL and their $\pm 1\sigma$ experiment standard deviation uncertainties. The thin black lines show the effect of the theoretical uncertainties σ_{theory} on the signal cross section.